

1 **Characterising beach intertidal bar systems using multi-annual LiDAR**
2 **data**

3

4 **Abstract**

5 Intertidal bars are common in meso-macrotidal low-to-moderate energy coastal
6 environments and an understanding of their morphodynamics is important from the
7 perspective of both coastal scientists and managers. However, previous studies
8 have typically been limited by considering bar systems two-dimensionally, or with
9 very limited alongshore resolution. This paper presents the first multi-annual study of
10 intertidal alongshore bars and troughs in a macro-tidal environment using airborne
11 LiDAR data to extract three-dimensional bar morphology at high resolution.

12 Bar and trough positions are mapped along a 17.5 km stretch of coastline in the
13 northwest of England on the eastern Irish Sea, using eight complete, and one partial,
14 LiDAR surveys spanning 17 years. Typically, 3 – 4 bars are present, with significant
15 obliquity identified in their orientation. This orientation mirrors the alignment of waves
16 from the dominant south-westerly direction of wave approach, undergoing refraction
17 as they approach the shoreline. Bars also become narrower and steeper as they
18 migrate onshore, in a pattern reminiscent of wave shoaling. This suggests that the
19 configuration of the bars is being influenced by overlying wave activity. Net onshore
20 migration is present for the entire coastline, though rates vary alongshore, and
21 periods of offshore migration may occur locally, with greatest variability between
22 northern and southern regions of the coastline.

23 This work highlights the need to consider intertidal bar systems as three-
24 dimensional, particularly on coastlines with complex configurations and bathymetry,

25 as localised studies of bar migration can overlook three-dimensional behaviour.

26 Furthermore, the wider potential of LiDAR data in enabling high-resolution

27 morphodynamic studies is clear, both within the coastal domain and beyond.

28 Key words: beach, intertidal bars, macrotidal, remote sensing, LiDAR, EOF analysis

29 **Introduction**

30 Intertidal bars are a defining morphological feature of many meso-macrotidal, low-to-

31 moderate energy coastal environments (van Houwelingen et al., 2008; Anthony et

32 al., 2007), where they fulfil an important role as sediment stores (Reichmüth &

33 Anthony, 2007). While their formation and evolution have been studied for many

34 years, following the pioneering work of King and Williams (1949), our understanding

35 remains limited. Improved understanding of the development of intertidal bar

36 systems will be beneficial to coastal managers, for whom the evolution of bars is a

37 key factor in controlling beach levels as well as an influence on sediment transport

38 within the intertidal zone.

39 A range of different intertidal bar system are found dependent upon beach

40 characteristics and hydrodynamic conditions. Some beaches may exhibit a single

41 bar whilst others may exhibit multiple bars; the maximum number of bars on a beach

42 varies depending upon tidal range, wave activity and beach gradient (Masselink et

43 al., 2006). Masselink et al. (2006) propose three main categories of intertidal bars

44 depending primarily upon wave conditions, tidal range and nearshore gradient. One

45 of these categories, which best represent the morphology considered in this paper, is

46 low amplitude ridges. These are shore parallel bars, typically occurring in groups of

47 2-6 and intersected by shore-parallel drainage channels. They form on low gradient

48 beaches with low to moderate wave energy and a meso- to macrotidal regime.

49 Generally, the number of bars present will increase as beach gradient and/or wave
50 activity decreases. Vertical, cross-shore and longshore scales of bar dimensions are
51 of order 0.5, 20 and 100 m respectively (Masselink et al., 2006), although
52 considerable variation may be observed.

53 The most important processes acting on bars are those resulting from the dissipation
54 of wave energy (Masselink et al., 2006), which results in bar crests being a focus for
55 sediment transport (Cartier and Hequette, 2013). Incident waves undergo
56 transformation processes including shoaling, breaking, reflection and refraction
57 (Wijnberg and Kroon, 2002) all of which will determine the resultant sediment
58 transport and thus the influence on beach morphology. While wave processes are
59 critical to bar development, intertidal bars will experience significant modulation in
60 the importance of different wave processes throughout the tidal cycle (Masselink et
61 al., 2006). These can be considered in relation to the relative tidal range (RTR),
62 which is the ratio between tidal range and significant wave height. A larger RTR,
63 indicating a large tidal range and small waves, results in shorter residence time for
64 swash and surf zone processes and an increased importance of wave shoaling,
65 leading to greater variation in the direction of sediment transport. This generally
66 leads to onshore migration of bars during low energy conditions, with flattening and
67 offshore migration of bars during high energy conditions (Kroon & Masselink, 2002).
68 However, other factors may influence the effect a particular wave condition will have
69 on bar development, including wave angle and water depth at the bar crest (Walstra
70 et al., 2012). Consequently, a wave of a particular height and period may drive either
71 onshore or offshore bar movement and bar growth or decay, depending upon the
72 combination of water depth and wave angle. In some locations, it has been noted
73 that bar migration may occur consistently in one direction under a wide variety of

74 prevailing conditions (Jackson et al., 2016). Alongshore sediment transport can also
75 be significant in these systems, particularly within troughs due to longshore currents
76 over the tidal cycle (Masselink et al., 2006). A number of studies have suggested
77 that changes in bar systems are predominantly two dimensional, occurring in the
78 form of a cross-shore redistribution of sediment (Houser and Greenwood, 2007;
79 Masselink et al., 2008). However, few studies undertaken to date possess the spatial
80 or temporal extent to enable identification of long-term changes in three-dimensional
81 bar morphology (Grunnet and Hoekstra, 2004).

82 Longer term 3D bar evolution is challenging to study in detail due to the logistical
83 difficulties inherent in obtaining high resolution measurements over large temporal
84 and spatial scales (annual to decadal and 10s kilometers respectively). Beach profile
85 surveys (e.g. Masselink & Anthony, 2001) are typically carried out several times a
86 year and allow changes in beach volume and morphology to be calculated (Smith
87 and Zarillo, 1990). However, profiles can only be taken at limited locations due to
88 time and cost restrictions. Profile spacing for long term monitoring is typically of order
89 500 m – 1 km (Masselink and Anthony, 2001), which is sufficient to detect large
90 scale trends in the evolution of coastal morphology but not to detect the detailed
91 three-dimensional evolution of morphological features such as bars, and potentially
92 misses important local changes. To the authors' knowledge, very few studies have
93 addressed longshore bar variability, an exception being Reichmüth & Anthony
94 (2008), who also examined low-amplitude ridges on a macrotidal beach using a
95 number of beach profiles over a period of c. 1 year. Grunnet & Hoekstra (2004) use
96 a rare set of beach profile surveys with a large spatial (12 km at 200 m intervals) and
97 temporal (28 years at annual intervals) extent to examine bar variability, but the
98 study covers nearshore rather than intertidal bars.

99 Airborne LiDAR offers a solution to the problem of spatial extent and resolution, by
100 providing rapid coverage of large areas of coastline at horizontal resolutions of up to
101 25 cm and vertical accuracies of order 15 cm (Sallenger et al., 2003), and modern
102 systems improve on this further with horizontal and vertical accuracies of order 10
103 cm (Andersen et al., 2017). As a result, LiDAR is increasingly being used as a tool
104 for monitoring coastal change around the world. One of the main limiting factors is
105 the cost, which is usually in the order of tens of thousands of pounds for a stretch of
106 coastline. However, the cost of surveys continues to fall and some regions are
107 already covered by a substantial time series of LiDAR surveys, although it is still
108 accepted that LiDAR datasets must be supplemented with additional data in order to
109 effectively study shorter term processes (Priestas and Fagherazzi, 2010). From
110 2016, the U.K.'s Open Government Initiative resulted in extensive catalogues of
111 LiDAR data being made freely available for large parts of England and Wales,
112 providing coverage of many coastal regions (Matthew, 2015).

113 A single LiDAR survey can provide valuable three-dimensional information on
114 coastal morphology which cannot easily be determined using traditional survey
115 methods. Saye et al. (2005) used LiDAR to calculate beach parameters including
116 height of the most seaward frontal dune ridge, frontal dune volume, beach volume,
117 beach width and average beach slope. They estimated that with the 15 cm vertical
118 accuracy of the LiDAR data, the error in the calculated parameters would range from
119 ~1% to 6% depending upon beach 'thickness' (its height relative to the survey
120 datum). A number of more recent studies have extracted beach parameters from
121 LiDAR data including dune toe and crest positions (Houser et al., 2008, Pye and
122 Blott, 2016, Stockdon et al., 2009) and shorelines (Houser et al., 2008, Liu et al.,
123 2007, Robertson et al., 2004). As with Saye et al (2005), Stockdon et al. (2009)

124 extracted profiles from the LiDAR digital elevation model (DEM) which in turn were
125 used to calculate relevant beach parameters, in this case dune crest location. This
126 technique allows for analysis usually applied to traditional beach profiles to be
127 applied to LiDAR data, while benefitting from the greatly improved resolution that
128 LiDAR provides. Houser & Mathew (2011) fully exploited this, extracting 2000
129 profiles from a single LiDAR survey, which covered 40 km of shoreline at 20 m
130 intervals. Such results could not feasibly be achieved using traditional ground-based
131 survey techniques.

132 While the application of LiDAR data has tended to focus on the analysis of dune
133 systems or whole intertidal beach volumes, the resolutions and vertical accuracy
134 also allows for analysis of smaller scale features such as sandbars. A few studies
135 have exploited this to date; van Houwelingen et al. (2006) utilised a single LiDAR
136 survey in order to analyse intertidal bars in North Lincolnshire, UK, whilst Levoy et. al
137 (2013) utilised 2.5 years of LiDAR data in their study of transverse bars and
138 concluded that tidal currents alone were sufficient to drive bar migration in the
139 absence of waves. LiDAR data are well suited to the study of intertidal bars due to
140 their high level of accuracy in x, y and z dimensions and the presence of a growing
141 archive of coastal LiDAR data available for analysis. Long term monitoring of bar
142 systems is necessary because long term nonlinearities in bar evolution can make bar
143 behaviour hard to predict (Pape, 2010).

144 This paper provides the first study of intertidal bars using high-resolution airborne
145 LiDAR surveys, allowing for a detailed consideration of three-dimensional bar
146 morphology and its evolution over time. The questions that this paper aims to answer
147 are:

148 • How does the bar system vary cross-shore and alongshore?

149 • How does the bar system evolve in time?

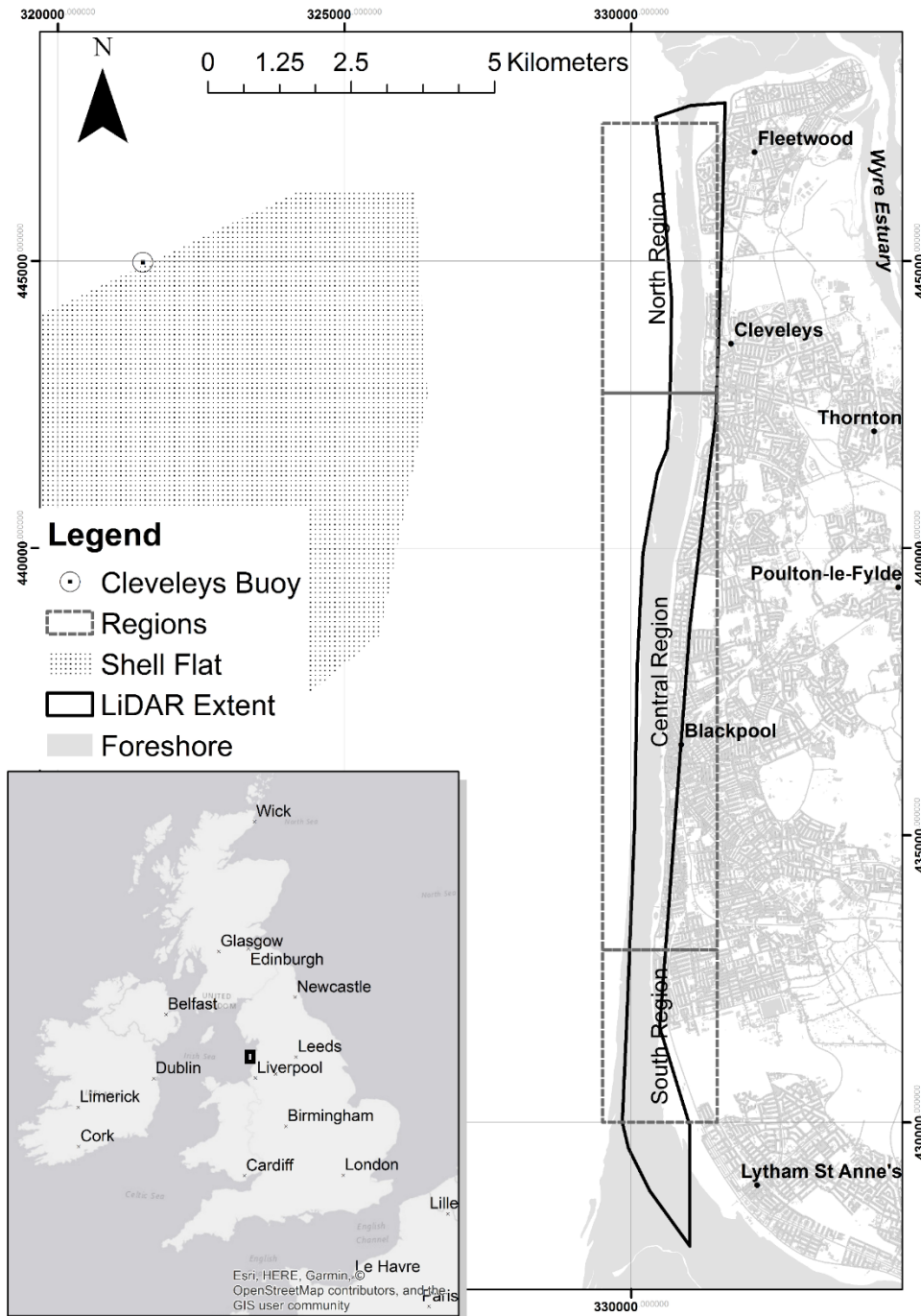
150 These will be answered through detailed analysis of LIDAR data in terms of the
151 degree of spatial and temporal variability of the geomorphic bar parameters. Eigen
152 function (EOF) analysis will be applied to extract common spatial bar behaviour
153 along the large stretch of coast and determine the degree of variability. The focus of
154 this study will be the Fylde coast, U.K., an area for which multiple LIDAR datasets
155 are available, and in which the bars have been subject to previous study using
156 traditional methods (King and William, 1949; Masselink and Anthony, 2001 and de
157 Alegria Arzaburu et al. 2007).

158 **Study Area**

159 The Fylde coast is located in the northwest of England fronting on to the Irish Sea
160 basin. The study area covers the entire western facing section of the coastline
161 extending over 17.5 km (Figure 1). The southern 1.6 km of the study area is backed
162 by a natural dune system (Figure 1, South Region). North of this, the area is fronted
163 by sea walls (Figure 1, Central Region), with groyne fields located in the northern 6
164 km (Figure 1, North Region). These defences are primarily to provide flood
165 protection to the low-lying hinterland, in particular for the adjacent resort towns of
166 Cleveleys and Blackpool, where properties are less than 10 m above Ordnance
167 Datum (AOD) (Figure 1). The structures also help to maintain beach levels, which
168 are a significant asset to the tourist industry in the region. The structures vary
169 significantly in age, construction and state of repair, with the earliest defences dating
170 back to the 1920s through to a new scheme to the north of Cleveleys, which would
171 have been under construction during the 2016 LiDAR survey, the most recent

172 included in this paper. Many of the groynes are in a poor state of repair, limiting their
173 effectiveness, although several recent rock groynes form effective barriers to
174 longshore sediment transport.

Figure 1 TOP



175

176 **Figure 1 Study area location map showing locations of interest**

177 The coastline experiences a macrotidal regime, with a mean spring tidal range of 8.0
178 m and a storm surge of over 1.0 m. It is fetch limited from all directions due to the
179 sheltering influence of Ireland to the west, the Isle of Anglesey on the Welsh
180 coastline to the south and the Isle of Man to the northwest, resulting in a maximum
181 fetch of approximately 375 km from the southwest. Based on data collected by a
182 Datawell Directional WaveRider Mk III buoy located offshore of the study site (Figure
183 1) and provided by the Channel Coast Observatory, the mean wave height was 0.6 –
184 1.5 m, wave period was 4 – 6 s and direction was 218 – 255°, during the period of
185 June 2011 – April 2016, although the wave direction in particular demonstrates a
186 great deal of variability. The beach is characterised by a multiple intertidal bar
187 system, usually consisting of 2 – 3 bars, and is one of the archetypal ridge and
188 runnel beaches as classified by King & Williams (1949). These will be referred to as
189 bars or inter-tidal bars throughout the study. The beach is largely sandy but a shingle
190 upper beach is also present along some sections (Pye et al., 2010).

191 **Methods**

192 This study is based on a time-series of 9 LiDAR datasets available for the Fylde
193 coast, spanning 17 years from 1999 to 2016 (Table 1). It is important to note that
194 there is substantial variability in the temporal spacing between surveys, varying from
195 3 months up to 9 years and 10 months. The LiDAR datasets were provided as post-
196 processed and quality checked gridded digital elevation models (DEMs), at
197 resolutions ranging from 0.25 m to 2.00 m by the Environment Agency's Geomatics
198 Group in partnership with the Cell 11 Regional Monitoring Strategy (CERMS).

199

200

201 **Table 1 Dates and resolutions of LiDAR survey data**

Name	Year	Month	Resolution (m)
1999	1999	March	2
2008	2008	December	1
2009	2009	March	0.25
2010	2010	January	1
2011	2011	March	2
2013a	2013	January	2
2013b	2013	November	1
2014	2014	February	2
2016	2016	April	1

202

203 **Bar Extraction Techniques**

204 The spatial density of LiDAR data allows for analysis of longshore variability of bar
 205 parameters and three-dimensional changes that have occurred between surveys. In
 206 order to automate the identification of bar locations, a series of profiles were
 207 extracted from the LiDAR dataset at a cross-shore and longshore resolution of 2 m.

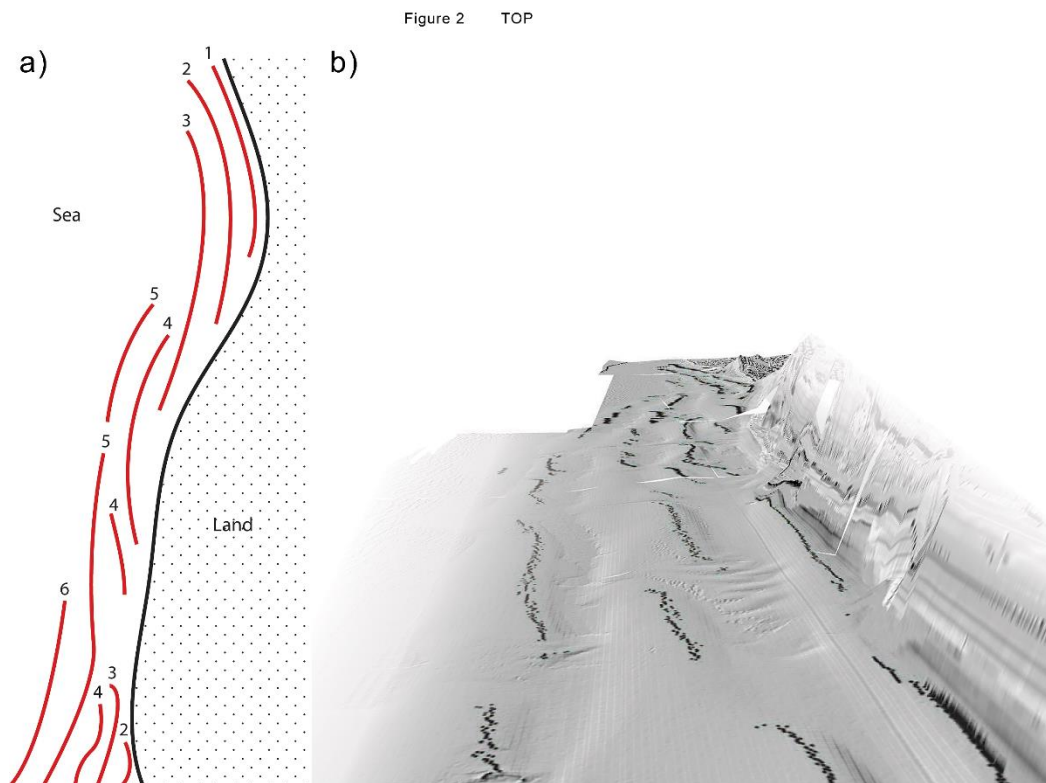
208 The crest positions of bars were extracted from the profiles using an algorithm
 209 written in the R programming language to determine peaks and troughs in the profile,
 210 based on the change in slope from positive to negative¹.

211 In order to effectively visualise the data and assess data quality, the resultant crest
 212 and trough locations were imported in to GIS software (ESRI ArcGIS 10.2) where
 213 they were overlaid on the original LiDAR elevation data (Figure 2b). Erroneous bar
 214 crest points, which occur due to the presence of manmade structures, gaps in the
 215 dataset or the presence water in the survey extent, were manually removed. A

¹ R code available at <https://gist.github.com/dgromer/ea5929435b8b8c728193>

216 numbering system was then applied to points in both crests and troughs in order to
217 designate the bar structure to which they belonged; the first crest was considered to
218 be offshore of the first trough; a schematic of the numbering system for bar crests is
219 shown in Figure 2a. Bars were considered to be continuous even when bisected by
220 drainage channels if they continued to occupy a similar cross-shore position either
221 side of the break.

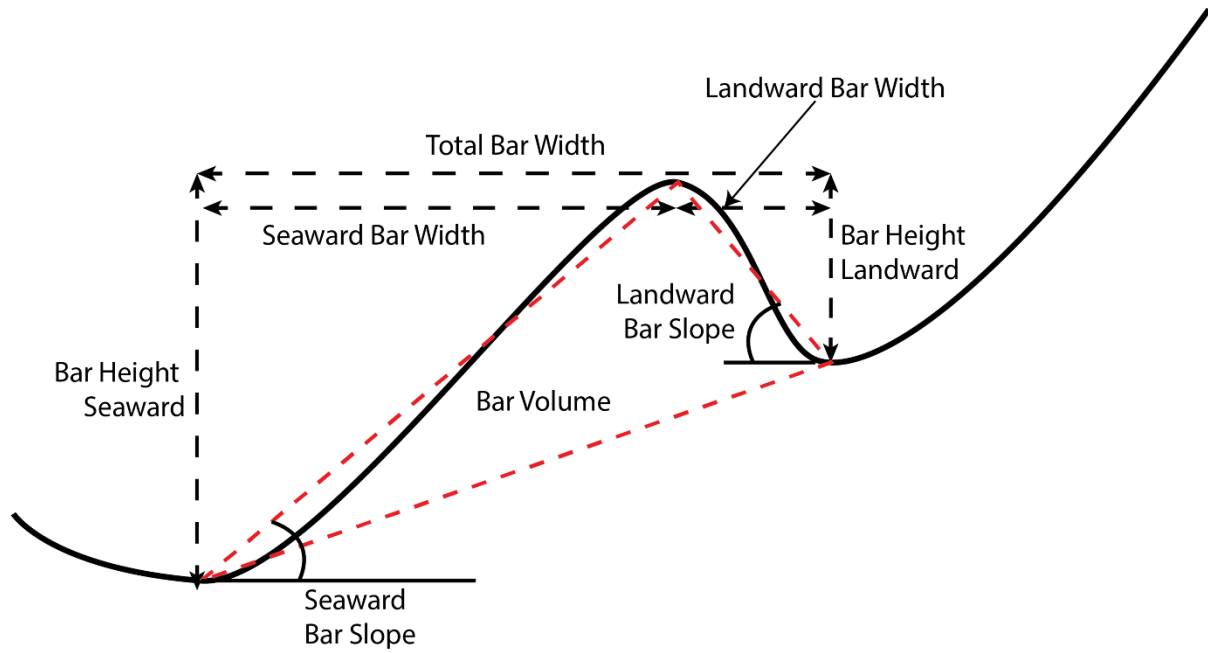
222 Finally, the positional attributes (location and elevation) of adjacent bar crests and
223 troughs were used to calculate a wider range of bar parameters including bar width,
224 bar slope and bar volume (Figure 3). These could then be used to determine
225 longshore and cross-shore variability in the bar system, as well as temporal
226 variability throughout the study period when compared between surveys.



227

228 **Figure 2 a) Schematic of the bar crest and trough numbering system used along the Fylde coast. This**
229 **numbering system is used as reference to bar position (e.g. inner, middle, outer bar) and may result in a**
230 **bar being given different designations at different points along the coast b) a 3D representation of actual**
231 **bar crests extracted from the airborne LiDAR data**

Figure 3 TOP



232

233 **Figure 3 Bar parameters calculated using bar crest and trough positions. Heights and widths are**
234 **measured in metres (m), bar volume in m³/m, slopes are calculated as a ratio.**

235 **EOF Analysis**

236 EOF analysis has been used by a number of authors to examine the spatial and
237 temporal evolution of beach morphology (Miller and Dean, 2007, Pruszek, 1993).
238 The datasets used have largely been generated from widely spaced beach profiles,
239 rather than the high-resolution dataset used in the current study, however the
240 principles remain the same. Partially due to this low spatial resolution, many previous
241 studies have also focused on analysis of temporal rather than spatial variability,
242 although some have also attempted to consider the spatial component (Dick and
243 Dalrymple, 1985, Miller and Dean, 2007). EOF analysis aims to concisely summarise
244 complex datasets into a number of numerical functions (eigenfunctions), with each
245 function describing a component of the variability within the dataset. Typically the
246 first three eigenfunctions explain in the order of 90% of the total variability. As EOFs
247 have a statistical rather than physical basis, coupling the results to physical
248 descriptions of the coastline can be challenging (Kroon et al., 2008). However,

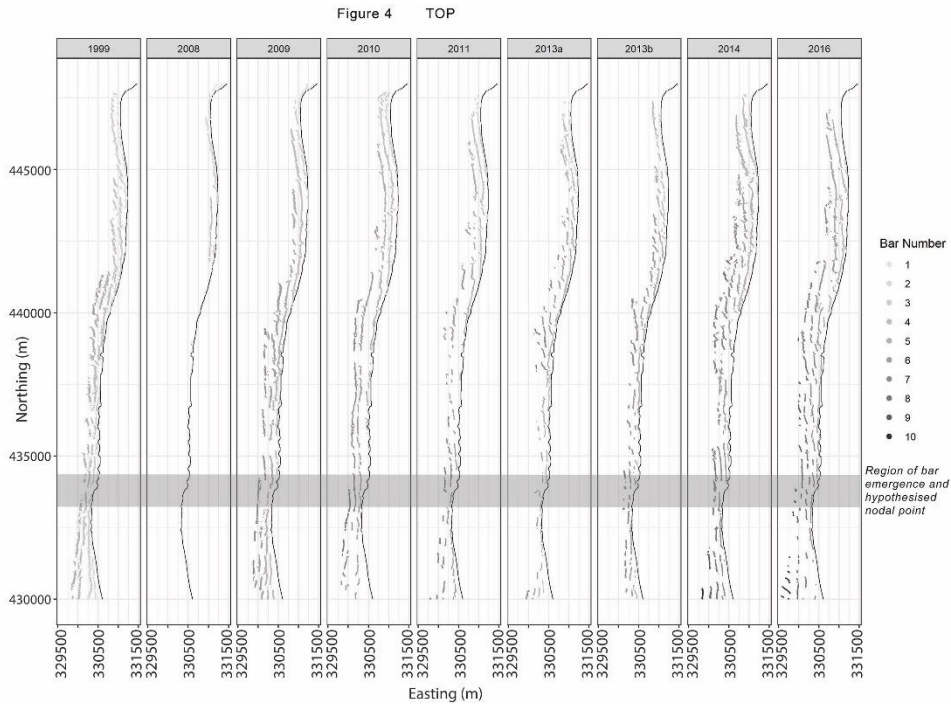
249 previous studies have identified that when analysing beach topography, these first
250 three functions typically relate well to particular physical attributes of the beach. The
251 first function identifies the mean beach profile, the second is a 'rotation factor' that
252 relates to variation in the mean profile alongshore and the third represents significant
253 morphological features present on top of the mean profile (Larson et al., 2003; Miller
254 & Dean, 2007). In the case of a barred beach, this will be the bars themselves and
255 will therefore be of greatest interest within the current study.

256 EOF analysis requires a rectangular matrix of data on which to operate, so the
257 coastline data were transformed by converting geographic eastings to chainage,
258 beginning from the toe of the seawall or dune system as appropriate (Dick and
259 Dalrymple, 1985). Analysis was limited to the upper 250 m of the beach because,
260 due to variability in beach slope, and therefore width, any greater extent would result
261 in areas of no data being present within some of the LiDAR datasets. This upper 250
262 m region typically includes the innermost two bars at any given section of coastline.

263 **Results**

264 **Bar Crest Parameters**

265 Examination of the bar crest positions extracted from airborne LiDAR (Figure 4)
266 provide a number of insights regarding large scale bar configuration. The first is that,
267 although intersected by frequent drainage channels, the bars themselves can be
268 considered continuous over large distances, in some cases extending well over 10
269 km. The bars emerge in the intertidal region first around a northing of 434000,
270 towards the south of Blackpool (Figure 4). However, their alignment with the
271 coastline is not shore parallel, with obliquity of the bars both north and south of this
272 location.



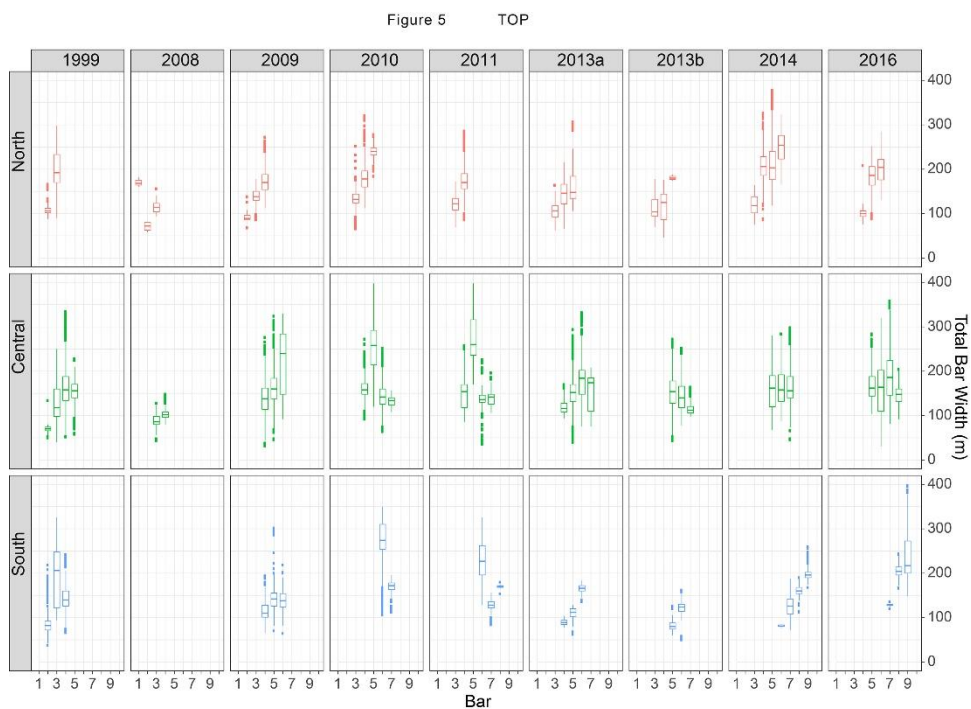
273

274 **Figure 4 Bar crest positions extracted from airborne LiDAR data**

275 Bar migration can be seen to be generally onshore over time, with bars emerging
 276 from offshore and ultimately dissipating as they merge with the upper beach. Some
 277 periods of offshore bar migration are also observed, particularly in the southern
 278 region of the coastline between 2011 – 2013a and 2014 - 2016. Due to the obliquity
 279 noted previously, a bar will occupy different cross-shore positions at different
 280 locations alongshore. As a result, a particular bar may occupy the most onshore
 281 position and be in the process of merging with the upper beach at the end located
 282 closest to the nodal point. Meanwhile, the end most distant from the nodal point
 283 could be located several hundred meters from the upper beach, and with two other
 284 bars located onshore of it. These variations in position will also correlate with the
 285 morphology of the bar, including width and steepness, which will be addressed in
 286 subsequent sections.

287 Analysis of the coastline was split into three regions, north, central and south (Figure
 288 1) in order to investigate the variability of bars alongshore. Figure 5 presents bar

289 widths across time and region for each bar. The most obvious pattern is that the bars
 290 located closer to land in each region tend to be the narrowest, suggesting they
 291 become progressively narrower as they migrate onshore. There is some indication
 292 within the central region that bars occupying central positions on the beach are
 293 widest, with narrower bars both onshore and offshore of this position – this is
 294 particularly apparent in 2010, 2011 and 2013a (Figure 5). The wider bars also
 295 demonstrate greatest variability in bar width, whether located offshore or more
 296 centrally on the beach, with mean bar width reaching in excess of 250 m and a range
 297 of almost 150 m between the upper and lower quartiles. Inner bars often approach
 298 100 m in width, with negligible variability.



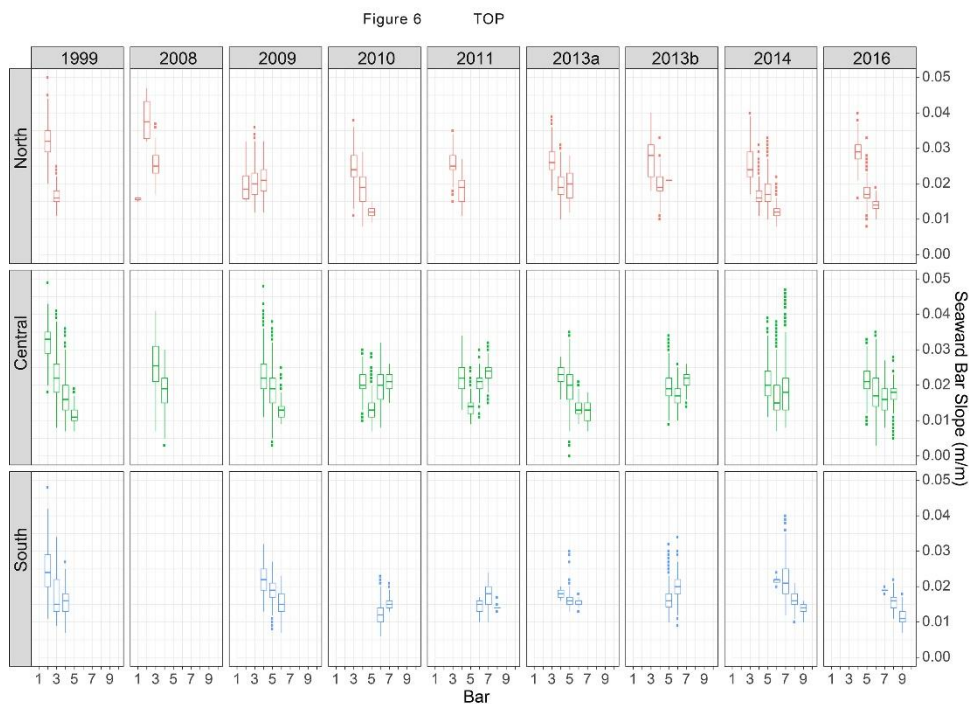
299

300 **Figure 5 Bar and whisker plot of bar width**

301 Concurrent with this narrowing of the bars is also a steepening as they migrate
 302 onshore (Figure 6). As well as being generally steeper, the more onshore located
 303 bars also show greater variability in the steepness. There are a few instances when
 304 this is not the case and the innermost bar shows extremely low variability,

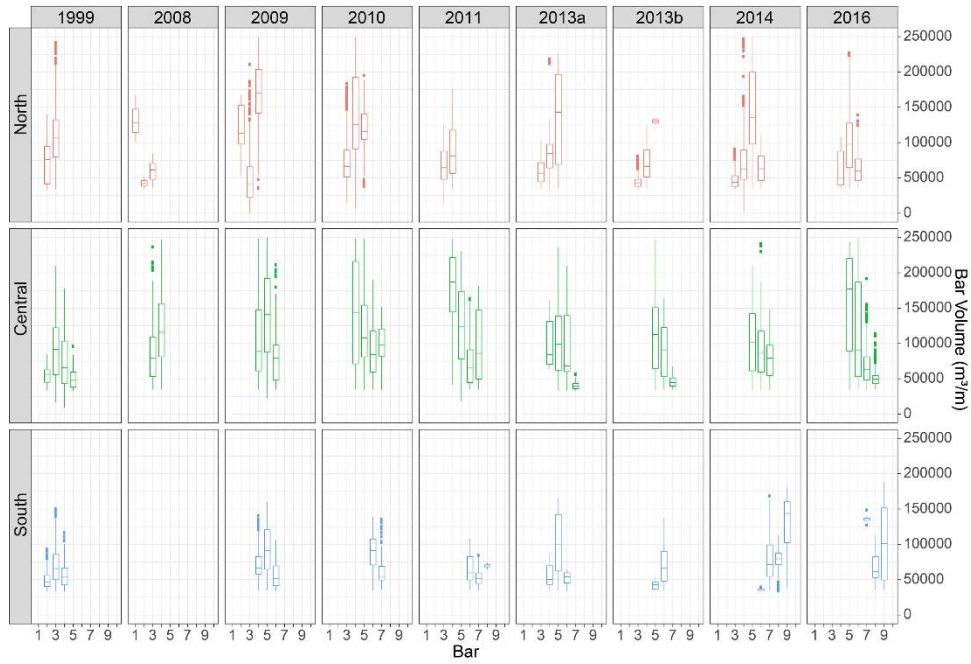
305 sometimes coupled with a drop in steepness; for example, the northern region in
306 2009 or the southern region in 2013a and 2014. However, this corresponds to times
307 when only a very small section of bar remains as it merges with the upper beach,
308 therefore reducing the opportunity for variability. Mean slope of the seaward bar face
309 varies between ~ 0.03 for steep inner bars to ~ 0.01 for the shallower outer bars.

310 The most variable parameter was found to be bar volume (Figure 7), a function of
311 both the width and height of the bar (Figure 3). It is important to note that this
312 pertains to the volume per meter length of the bar, rather than the volume of the bar
313 as a whole. It is therefore independent of the length of the bar, which would
314 otherwise be the most significant factor in determining volume.



316 **Figure 6 Bar and whisker plot of the slope of the seaward bar face**

Figure 7 TOP



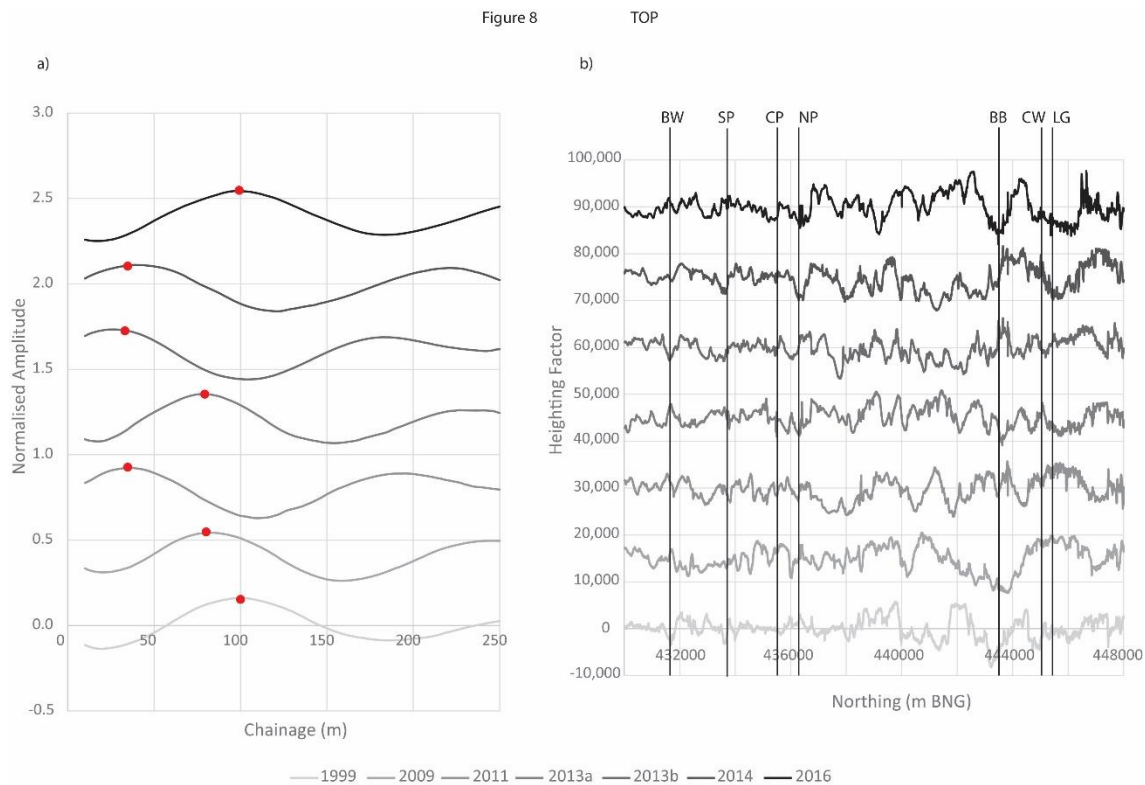
317

318 **Figure 7 Bar and whisker plot showing bar volumes broken down by year and region (refer to Figure 1 for**
319 **region extents).**

320 **EOF Analysis**

321 The results of EOF analysis follow the pattern identified by previous authors, with the
322 first three eigenfunctions representing mean profile, rotation factor and mean shape
323 and location of bars respectively. Here, we focus on bar shape and location (the third
324 eigenfunction, Fig 8). Typically, two bars are located within the upper 250 m of the
325 beach; the exceptions are 1999 and 2016, which both see the innermost bar located

326 at around 100 m chainage, and the crest of the second bar falling outside of the 250
 327 m region analysed.



328

329 **Figure 8 a) Results of the third eigenfunction, representing intertidal bars, offset vertically for 10-250 m**
 330 **chainage along the entire coastline. Points on lines indicate possible preferential bar locations. b)**
 331 **Vertically offset longshore coefficients for the third eigenfunction. BW = start of Blackpool seawall, SP =**
 332 **South pier location CP = Central Pier location, NP = North Pier location, BB = Blackpool and Cleveleys**
 333 **borough boundary CW = end of Cleveleys sea wall LG = location of extended groyne**

334 The third eigenfunction indicates that the inner bar may position itself around one of
 335 several preferential cross-shore locations, with clusters at around 100 m (1999 and
 336 2016), 80 m (2009, 2013a) and 35 m (2011, 2013b, 2014) (Figure 8a). Clustering is
 337 less obvious for the second bar crest, which are distributed between 175 m chainage
 338 out beyond 250 m. Narrowing and steepening of bars positioned further onshore,
 339 previously identified from analysis of the bar parameters, is clearly highlighted by the
 340 third eigenfunction, with the inner bar visibly steeper and narrower than the second
 341 bar in all cases. Analysis of beach profile data demonstrates that areas in which the
 342 coefficient of the eigenfunction is most variable also demonstrate the greatest

343 variability in beach profile envelope, further supporting the hypothesis that the third
344 EOF represents the bars.

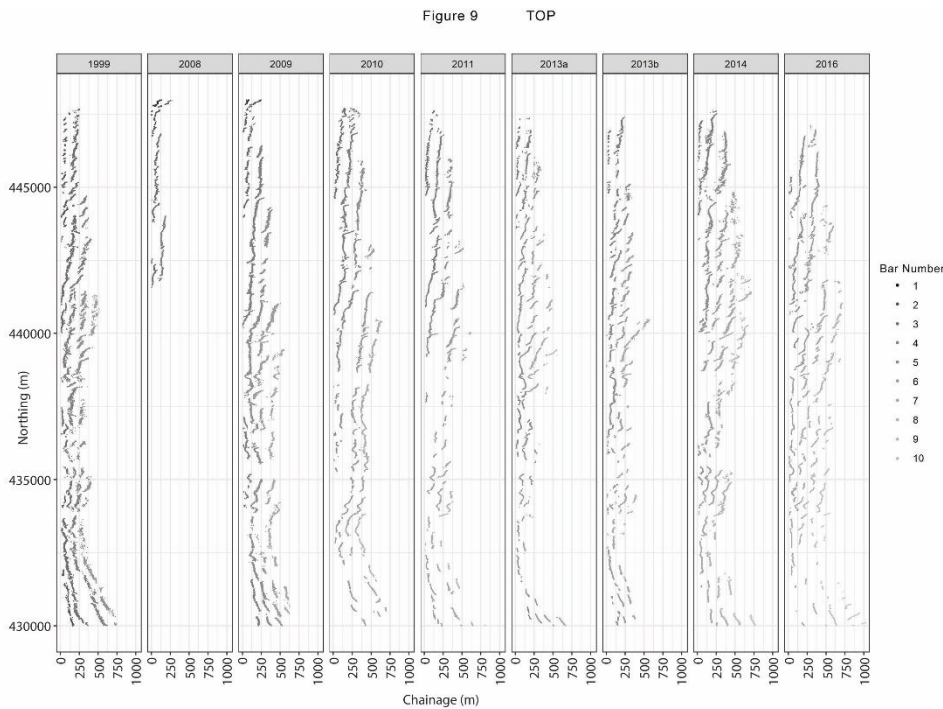
345 The coefficient of the eigenfunction provides an indication of its variation alongshore.
346 The coefficient for the third eigenfunction is typically quite complex and is shown in
347 Figure 8b. This highlights the alongshore variability of the bars themselves. The
348 largest variations at scales of 1000s of meters are observed in the northern part of
349 the beach and are more pronounced in 2009, 2014 and 2016. Small scale variations
350 at scales of 100s and smaller are also observed, demonstrating high variability from
351 year to year and are related to the location of groynes and drainage channels.

352 **Discussion**

353 ***Bar configuration***

354 Bars are generally obliquely oriented towards the shoreline, which is evident from all
355 LIDAR surveys. The idea that bar obliquity to the shoreline influences the observed
356 pattern of evolution has been identified as far back as King (1972), although the bars
357 in the Fylde Coast region have typically been treated as shore-parallel. In fact, when
358 the Fylde coast is considered in its entirety, bars appear to approach the shoreline
359 first towards the south of the region, at a northing of around 434000 (Figure 1), and
360 then extend obliquely from the shoreline in both directions away from this point. This
361 behaviour is consistent with previous studies in the region which have identified the
362 existence of a nodal point in longshore sediment transport somewhere in this vicinity
363 (Halcrow, 2010). The obliquity in the bar system away from this point is enhanced by
364 the embayed shape of the coastline, which would require rotation of the bar system
365 to achieve a shore-parallel alignment. Bar obliquity is highlighted further when bar
366 positions are visualised as a function of chainage, rather than geographical location

367 (Figure 9). From this perspective the more offshore bars demonstrate greater
368 obliquity, while more onshore bars have closer alignment with the coast, although
369 they never fully reach shore-parallel. It is hypothesized that this alignment mirrors the
370 alignment of waves from the dominant south-westerly direction of wave approach,
371 undergoing refraction as they approach the shoreline.



372

373 **Figure 9 Plot of bar positions as a function of chainage. The obliquity of the bars becomes more**
374 **apparent when the shape of coastline is removed, as does the greater alignment of innermost bars**
375 **compared to those located further offshore.**

376 While the obliquity of the bars away from the nodal point could be interpreted as
377 longshore translation of the bars as they migrate onshore, this overlooks the
378 influence that the bars themselves will have on longshore sediment transport both
379 through the influence on wave breaking and through flows in and out of the runnels
380 during flood and ebb tides, a feature of intertidal bar system previously highlighted by
381 Sedrati and Anthony (2007).

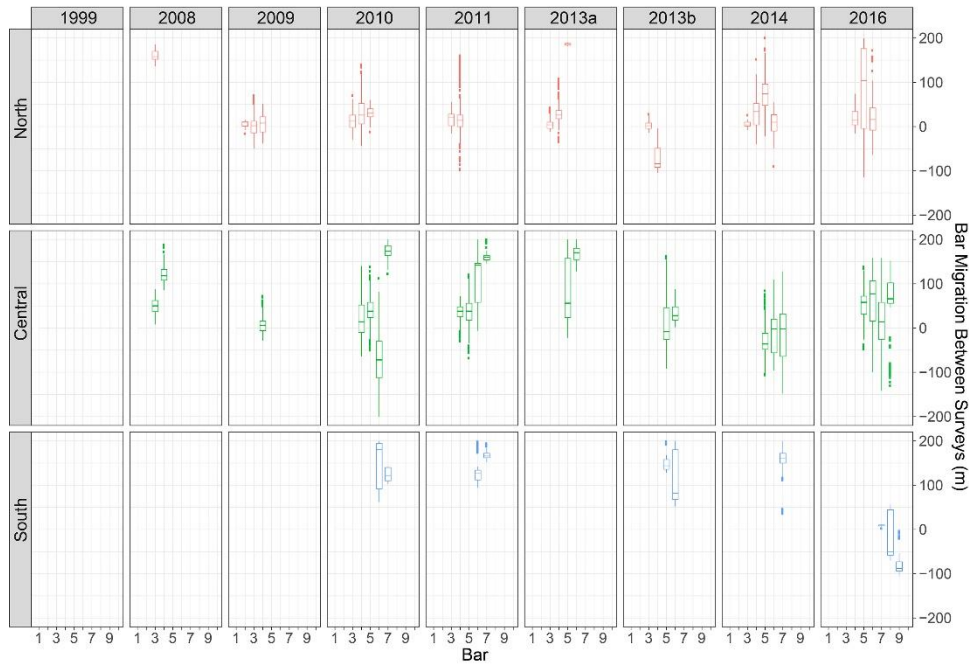
382 The number of bars observed is dependent upon the tidal level during LiDAR data
383 collection, but typically 3-4 bars are identified at any given location along the

384 coastline. The exception is the southernmost area in which no seawall is present,
385 resulting in a wider, shallower beach and significantly increasing the number of bars
386 observed to as many as seven. In a natural setting, it is expected that the number of
387 bars would similarly increase along the entirety of the coastline; in contrast, within
388 defended regions, spring high tide reaches above the base on the seawall, indicating
389 that the width of the beach is being artificially limited and the bar system is therefore
390 curtailed by its presence. Beach width does not appear to be limited by defenses at
391 the northern end of the coastline, where beach slope is steepest and fewer bars are
392 apparent; only two intertidal bars are ever present, as compared to 3-4 further south.
393 It is possible that sub-tidal bars are also present which cannot be observed in the
394 LiDAR data.

395 ***Bar Location***

396 Bar migration is seen to be typically onshore for all bars and regions of this coastline.
397 This is in agreement with analysis of the past beach profiles collected at Cleveleys
398 between 1991-2006 (de Alegria Arzaburu et al. 2007). The bars located furthest
399 offshore are most dynamic, with migration rates reaching over 100 m per year in
400 some instances (Figure 10). Bars located closest to shore have slower migration
401 rates of the order of 10 m per year, likely to be due to the innermost bars having
402 reduced exposure to wave activity, being submerged only during high tide
403 conditions.

Figure 10 TOP



404

405 **Figure 10 Bar and whisker plot of bar migration between surveys broken down by year and region (refer**
 406 **to Figure 1 for region extents). Positive values indicate onshore migration and negative offshore.**

407 While onshore bar migration is dominant, periods of offshore movement are also
 408 detectable. Intertidal bars have previously been shown to migrate offshore under
 409 more energetic conditions (Mariño-Tapia et al., 2007) and, therefore, movement
 410 between consecutive surveys may depend upon antecedent conditions. However,
 411 more frequent surveys would be required to investigate this effectively.

412 The net onshore migration has important implications for the sediment supply in this
 413 region, because it suggests that an offshore sediment source is providing the
 414 material for bar formation. Results also suggest that the cross-shore migration rate of
 415 the bar may vary alongshore, likely in response to variation in shoreline angle
 416 relative to wave direction. This will, in effect, lead to a rotation of the bar system and
 417 could also be a function of seasonal variability in wave height and direction.

418 It has previously been suggested that bars on Blackpool beach occupy a number of
 419 preferential positions across the profile (Masselink & Anthony, 2001), linked to the

420 residence times of wave driven processes at particular tidal elevations. However,
421 analysis of bar crest elevations in the present study indicates that they are
422 distributed evenly throughout the intertidal area. EOF analysis did suggest that the
423 innermost bar may occupy one of a number of cross-shore positions at a given time
424 based upon chainage. However, the obliquity of the bars and significant longshore
425 variability means that any preferential positions are likely to be highly localised. It is
426 possible that the same may be true for bar crest elevations, and that binning of the
427 data into finer longshore sections would result in preferential bar positions emerging
428 at a local scale. However, on the scale of the whole Fylde coast there is no evidence
429 for this, and bars appear to progress steadily onshore.

430 ***Bar Parameters***

431 One of the most significant observations from the calculation of bar parameters is the
432 narrowing and steepening which occurs as bars move onshore, reminiscent of wave
433 shoaling. The relative duration of the wave processes each bar is exposed to are
434 likely to be key to this evolution, varying over the course of the spring-neap tidal
435 cycle (Masselink et al., 2006). Analysis of several profiles from the Fylde Coast was
436 carried out to determine the residence times of wave shoaling, breaking and swash
437 processes during spring and neap tidal conditions. During spring tidal conditions,
438 wave processes migrate most rapidly across the profile and, under typical low
439 energy conditions, wave shoaling will dominate across all bars, resulting in onshore
440 sediment transport. Under storm conditions, wave breaking will play a more
441 significant role over the inner two bars. During neap tidal conditions the duration of
442 wave processes over the bars will increase. Under low energy wave conditions, the
443 inner bar will be dominated by swash processes, resulting in onshore sediment
444 transport and providing a possible mechanism for bar steepening. Subsequent bars

445 will experience a combination of shoaling and breaking and may undergo very little
446 morphological change. Under energetic wave conditions all bars except the
447 innermost will be dominated by offshore directed sediment transport. In summary,
448 the inner bar will be dominated by onshore directed sediment transport, and as a
449 result has the appearance of a slip-face bar attached to the upper beach. When
450 combined with observations of bar crest orientation, which are oblique to the
451 coastline but become increasingly shore-parallel as they move onshore, this
452 suggests that the configuration of the bars is being influenced by overlying wave
453 activity.

454 The parameter which shows the most variability between regions is bar volume
455 (Figure 7). In the central region, it is often the innermost bar which has the greatest
456 volume, while in the northern region the outermost or central bars typically contain
457 the greatest volume. The southernmost region shows the greatest variation, with
458 outer, central and inner bars all being most voluminous at different points in time.

459 From the analysis presented here, there are significant differences in beach
460 parameters along the studied coastline. These variations can be attributed to two
461 major influences. The first is the coastal configuration, e.g. gentle embayment
462 /headland like structure in the central and northern sections. The second is due to
463 presence of coastal structures such as piers (extending up to 350m offshore),
464 groynes (extending up to 100m) and artificial headlands (extending up to 50m),
465 which directly impact on the configuration of the bar system. These tend to have a
466 persistent impact on alongshore variability across the years, although their
467 contribution to the Eigen coefficient is still variable. This may explain the greater
468 variability in the northern 5 km of the coastline where a groyne field is present. In
469 addition, the presence of cross-shore drainage channels is mirrored in variations at

470 smaller spatial scales. These channels are frequent, occurring every few hundred
471 meters alongshore, and highly dynamic, forming and migrating on timescales which
472 cannot be tracked using annual LiDAR surveys (Miles, 2014; Reichmüth & Anthony,
473 2008). It is the presence of these channels which makes the alongshore EOF
474 coefficients so varied year on year.

475 While hydrodynamics have not been studied here, the shape and orientation of bars
476 indicate a probable causal relationship between waves and bars. Nearshore wave
477 transformation will be influenced by shoreline configuration and orientation as well as
478 nearshore bathymetry and the bars themselves. The Shell Flat (Figure 1), is a
479 shallower offshore area attached to the northern part of the Fylde coast. Wave
480 energy will be transformed around the flat before reaching the adjacent nearshore
481 zone. Hence it is expected that larger wave heights will be found on the central and
482 southern part of the coastline. This is supported by the tracking of bar migration
483 rates, which are typically greater in the southern region of the coastline than in north
484 or central. While the bars are influenced by wave characteristics, the oblique angle of
485 the bars will itself result in a variation in longshore slope which, alongside shoreline
486 orientation with respect to incident waves, will provide gradients in longshore
487 sediment transport.

488 The results presented here are in agreement with those of Grunnet and Hoekstra
489 (2004) who analysed longshore bar variability from beach profiles at Terschelling,
490 the Netherlands, highlighting the influence of coastal configuration and bathymetry
491 on bar parameters and migration, albeit with a longshore resolution limited to a
492 maximum of 200 m. Hence, we argue that our study has much wider relevance
493 highlighting a need for 3D study of bars and in particular on coastlines with more
494 complex configuration and bathymetry. Localised studies of bar migration can be

495 misleading, overlooking three-dimensional behavior of the bar system. In particular
496 the obliquity of the bars cannot easily be determined from discrete profiles.

497 **Limitations**

498 A number of gaps in the knowledge remain following the work in this paper, which
499 largely revolve around understanding of the short-term (hourly to weekly) evolution of
500 the bar system between available LiDAR surveys. This may be addressed by a
501 combination of beach profile surveys, video monitoring and numerical modelling of
502 the nearshore environment. Considering short-term processes will also allow for
503 clearer links to be drawn between changes to the bar system and the hydrodynamic
504 processes responsible for them, which currently remain largely hypothesised. This
505 will also increase the value of the work from a coastal management perspective,
506 enhancing understanding of the impact which the bar system has on both sediment
507 transport and beach volumes.

508 Increasing the frequency of future LiDAR surveys to bi-annually would allow
509 researchers to capture variability between summer and winter conditions. Greater
510 consideration of tidal conditions, undertaking LiDAR surveys at or close to spring low
511 tide, would also help to ensure the maximum possible coverage of the intertidal
512 region. However, it is acknowledged that cost limitations make it unlikely that this will
513 be achieved in the near future.

514 **Conclusions**

515 The longshore variability and dynamics of an intertidal bar system have been
516 captured based upon nine airborne LiDAR surveys spanning the period 1999 – 2016.
517 The findings provide new insights into the configuration and dynamics of intertidal

518 bars on the Fylde coast and more widely. Of particular interest is the longshore
519 variability of the bar system over 10s kilometres, both in terms of dynamics and
520 morphology, something which is difficult to capture using traditional beach profile
521 surveys. It also demonstrates the potential of airborne LiDAR surveys for
522 morphological studies, not only of intertidal bar systems but also for other systems
523 operating on similar spatial and temporal scales.

524 The bars are found to first approach the coast at a nodal point in sediment transport.
525 The bars are then oriented obliquely to the coastline both to the north and south of
526 this location, with outermost bars demonstrating greater obliquity than those closer to
527 the shoreline. The migration rates of bars are found to vary alongshore and may
528 advance in some locations while retreating in others, resulting in a rotation of the bar
529 system. Typically, when such rotation occurs it is about the nodal point, with bars
530 migrating in different directions either side of the point. However, net migration for all
531 bars studied was onshore.

532 A substantial amount of the alongshore variability observed over time is due to the
533 presence of cross-shore drainage channels, which develop and migrate much more
534 rapidly than the bars themselves. This is demonstrated in the alongshore coefficient
535 of the third eigenfunction, representing bars, where frequent and highly variable
536 fluctuations are seen alongshore. Despite this, the third eigenfunction presents a
537 sound generalisation of the bar shape and position within the upper 250 m of the
538 coastline. The pattern of onshore migration is clear, as is the narrowing and
539 steepening of the bar occurring as it migrates onshore, in a fashion reminiscent of
540 wave shoaling.

541 This study has demonstrated the importance of considering intertidal bar systems as
542 three dimensional and studying them at an appropriate alongshore resolution in
543 order to fully capture and understand their morphology and evolution. Future LiDAR
544 surveys will allow for continued expansion of this work and improved understanding
545 of the long-term evolution of bar systems. Combining these findings with further
546 studies into short-term bar evolution, which should also consider their three-
547 dimensional nature, will greatly enhance our understanding of the dynamics of
548 intertidal bars and the influence they have on sediment transport and volumes.

549 **Acknowledgements**

550 The authors would like to thank Wyre Borough Council and the Environment
551 Agency for funding the research on which this study is based. They would also like to
552 thank the anonymous reviewers and associate editor of the journal for their helpful
553 and constructive comments.

554 **References**

- 555 Andersen MS, Gergely Á, Al-Hamdani Z, Steinbacher F, Larsen LR, Ernstsén VB. 2017.
556 Processing and performance of topobathymetric lidar data for geomorphometric and
557 morphological classification in a high-energy tidal environment. *Hydrology and Earth System
558 Sciences* **21**: 43
559
- 560 Anthony, E. J., Dussouillez, P., Dolique, F., Besset, M., Brunier, G., Nguyen, V. L., & Goichot,
561 M. 2017. Morphodynamics of an eroding beach and foredune in the Mekong River delta:
562 Implications for deltaic shoreline change. *Continental Shelf Research*. **147**: 155-164
563
- 564 Cartier A, Hequette A. 2013. The influence of intertidal bar-trough morphology on sediment
565 transport on macrotidal beaches, northern France. *Zeitschrift Fur Geomorphologie* **57**: 325-
566 347
567
- 568 Castelle B, Bonneton P, Dupuis H, Sénéchal N. 2007. Double bar beach dynamics on the
569 high-energy meso-macrotidal French Aquitanian Coast: a review. *Marine Geology* **245**: 141-
570 159
571

572 de Alegria Arzaburu, A. R., Ilic, S., & Gunawardena, Y. (2007). A study of intertidal bar
573 dynamics using the Argus video system. In *Coastal Sediments' 07* (pp. 1865-1876).
574
575 Dick JE, Dalrymple RA. 1985. Coastal changes at Bethany Beach, Delaware. In *Coastal*
576 *Engineering 1984*; 1650-1667.
577
578 Grunnet NM, Hoekstra P. 2004. Alongshore variability of the multiple barred coast of
579 Terschelling, The Netherlands. *Marine Geology* **203**: 23-41
580
581 Halcrow. 2010. Cell Eleven Tide and Sediment Transport Study (CETaSS) Phase 2.
582
583 Houser C, Greenwood B. 2007. Onshore migration of a swash bar during a storm. *Journal of*
584 *Coastal Research* **23**: 1-14
585
586 Houser C, Hapke C, Hamilton S. 2008. Controls on coastal dune morphology, shoreline
587 erosion and barrier island response to extreme storms. *Geomorphology* **100**: 223-240
588
589 Houser, C., & Mathew, S. 2011. Alongshore variation in foredune height in response to
590 transport potential and sediment supply: South Padre Island, Texas. *Geomorphology*, **125**:
591 62-72
592
593 Jackson DW, Cooper JAG, O'connor M, Guisado-Pintado E, Loureiro C, Anfuso G. 2016. Field
594 measurements of intertidal bar evolution on a high-energy beach system. *Earth Surface*
595 *Processes and Landforms* **41**: 1107-1114
596
597 King CAM, Williams WW. 1949. The Formation and Movement of Sand Bars by Wave Action.
598 *The Geographical Journal* **113**: 70-85
599
600 King, C. A. M. 1972. *Beaches and Coasts*. New York: St. Martin Press.
601
602 Kroon, A., & Masselink, G. 2002. Morphodynamics of intertidal bar morphology on a
603 macrotidal beach under low-energy wave conditions, North Lincolnshire, England. *Marine*
604 *geology* **190**: 591-608
605
606 Kroon, A., Larson, M., Möller, I., Yokoki, H., Rozynski, G., Cox, J., & Larroude, P. 2008.
607 Statistical analysis of coastal morphological data sets over seasonal to decadal time scales.
608 *Coastal Engineering*, **55**: 581-600.
609
610 Larson, M., Capobianco, M., Jansen, H., Rózyński, G., Southgate, H. N., Stive, M. & Hulscher,
611 S. 2003. Analysis and modeling of field data on coastal morphological evolution over yearly
612 and decadal time scales. Part 1: Background and linear techniques. *Journal of Coastal*
613 *Research* **19**: 760-775
614
615 Levoy F, Anthony EJ, Monfort O, Robin N, Bretel P. 2013. Formation and migration of
616 transverse bars along a tidal sandy coast deduced from multi-temporal Lidar datasets.
617 *Marine Geology* **342**: 39-52
618

619 Liu HX, Sherman D, Gu SG. 2007. Automated extraction of shorelines from airborne light
620 detection and ranging data and accuracy assessment based on Monte Carlo simulation.
621 *Journal of Coastal Research* **23**: 1359-1369
622

623 Mariño-Tapia I, O'Hare T, Russell P, Davidson M, Huntley D. 2007. Cross-shore sediment
624 transport on natural beaches and its relation to sandbar migration patterns: 2. Application
625 of the field transport parameterization. *Journal of Geophysical Research: Oceans* **112**:
626

627 Masselink G, Anthony EJ. 2001. Location and height of intertidal bars on macrotidal ridge
628 and runnel beaches. *Earth Surface Processes and Landforms* **26**: 759-774
629

630 Masselink G, Austin M, Tinker J, O'Hare T, Russell P. 2008. Cross-shore sediment transport
631 and morphological response on a macrotidal beach with intertidal bar morphology, Truc
632 Vert, France. *Marine Geology* **251**: 141-155
633

634 Masselink G, Kroon A, Davidson-Arnott RGD. 2006. Morphodynamics of intertidal bars in
635 wave-dominated coastal settings - A review. *Geomorphology* **73**: 33-49
636

637 Matthew A. 2015. Free mapping data will elevate flood risk knowledge. In *Environment*
638 *Agency Blog*. Environment Agency.
639

640 Miles A. 2014. Towards an understanding of intertidal forms and processes through
641 integrating field observations, remotely sensed data and hydrodynamic models. In *Lancaster*
642 *Environment Centre*. Lancaster University: Lancaster.
643

644 Miller JK, Dean RG. 2007. Shoreline variability via empirical orthogonal function analysis:
645 Part I temporal and spatial characteristics. *Coastal Engineering* **54**: 111-131
646

647 Pape, L., Kuriyama, Y., & Ruessink, B. G. 2010. Models and scales for cross-shore sandbar
648 migration. *Journal of Geophysical Research* **115**: F03043
649

650 Priestas AM, Fagherazzi S. 2010. Morphological barrier island changes and recovery of
651 dunes after Hurricane Dennis, St. George Island, Florida. *Geomorphology* **114**: 614-626
652

653 Pruszek Z. 1993. The analysis of beach profile changes using Dean's method and empirical
654 orthogonal functions. *Coastal Engineering* **19**: 245-261
655

656 Pye K, Blott S, Witton S, Pye A. 2010. Cell 11 regional monitoring strategy results of
657 sediment particle size analysis. Report (Kenneth Pye Associates Ltd.): 1
658

659 Pye K, Blott SJ. 2016. Assessment of beach and dune erosion and accretion using LiDAR:
660 impact of the stormy 2013–14 winter and longer term trends on the Sefton Coast, UK.
661 *Geomorphology* **266**: 146-167
662

663 Reichmuth, B., & Anthony, E. J. 2007. Tidal influence on the intertidal bar morphology of
664 two contrasting macrotidal beaches. *Geomorphology*, **90**: 101-114.
665

666 Reichmüth, B., & Anthony, E. J. 2008. Seasonal-scale morphological and dynamic
667 characteristics of multiple intertidal bars. *Zeitschrift für Geomorphologie, Supplementary*
668 *Issues*, **52**: 79-90.

669
670 Robertson WV, Whitman D, Zhang KQ, Leatherman SP. 2004. Mapping shoreline position
671 using airborne laser altimetry. *Journal of Coastal Research* **20**: 884-892

672
673 Sallenger AH, Krabill WB, Swift RN, Brock J, List J, Hansen M, Holman RA, Manizade S, Sontag
674 J, Meredith A, Morgan K, Yunkel JK, Frederick EB, Stockdon H. 2003. Evaluation of airborne
675 topographic lidar for quantifying beach changes. *Journal of Coastal Research* **19**: 125-133

676
677 Saye, S. E., Van der Wal, D., Pye, K., & Blott, S. J. 2005. Beach–dune morphological
678 relationships and erosion/accretion: an investigation at five sites in England and Wales using
679 LIDAR data. *Geomorphology* **72**: 128-155

680
681 Sedrati M, Anthony EJ. 2007. Storm-generated morphological change and longshore sand
682 transport in the intertidal zone of a multi-barred macrotidal beach. *Marine Geology* **244**:
683 209-229

684
685 Smith GL, Zarillo GA. 1990. CALCULATING LONG-TERM SHORELINE RECESSION RATES USING
686 AERIAL PHOTOGRAPHIC AND BEACH PROFILING TECHNIQUES. *Journal of Coastal Research* **6**:
687 111-120

688
689 Stockdon HF, Doran KS, Sallenger AH. 2009. Extraction of Lidar-Based Dune-Crest Elevations
690 for Use in Examining the Vulnerability of Beaches to Inundation During Hurricanes. *Journal*
691 *of Coastal Research* **25**: 59-65

692
693 Van Houwelingen S, Masselink G, Bullard J. 2006. Characteristics and dynamics of multiple
694 intertidal bars, north Lincolnshire, England. *Earth Surface Processes and Landforms* **31**: 428-
695 443

696
697 van Houwelingen S, Masselink G, Bullard J. 2008. Dynamics of multiple intertidal bars over
698 semidiurnal and lunar tidal cycles, North Lincolnshire, England. *Earth Surface Processes and*
699 *Landforms* **33**: 1473-1490

700
701 Walstra DJR, Reniers AJHM, Ranasinghe R, Roelvink JA, Ruessink BG. 2012. On bar growth
702 and decay during interannual net offshore migration. *Coastal Engineering* **60**: 190-200

703
704 Wijnberg KM, Kroon A. 2002. Barred beaches. *Geomorphology* **48**: 103-120

705

